



## Sugar apple-shaped TiO<sub>2</sub> hierarchical spheres for highly efficient dye-sensitized solar cells

Bing-Xin Lei, Li-Li Zeng, Ping Zhang, He-Kang Qiao, Zhen-Fan Sun\*

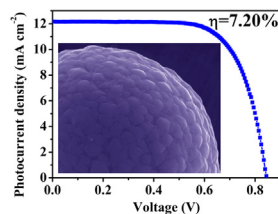
School of Chemistry and Chemical Engineering, Hainan Normal University, Haikou 571158, PR China



### HIGHLIGHTS

- The sugar apple-shaped TiO<sub>2</sub> hierarchical spheres were prepared by a facile hydrothermal method.
- The TiO<sub>2</sub> hierarchical spheres had a prominent light scattering effect.
- DSSCs based on TiO<sub>2</sub> double-layer film had the maximum conversion efficiency.

### GRAPHICAL ABSTRACT



### ARTICLE INFO

#### Article history:

Received 23 October 2013

Received in revised form

8 December 2013

Accepted 10 December 2013

Available online 18 December 2013

#### Keywords:

Titania

Microspheres

Light scattering

Hierarchical nanostructure

Dye-sensitized solar cells

### ABSTRACT

The sugar apple-shaped TiO<sub>2</sub> hierarchical spheres are prepared by a facile hydrothermal method using polyethylene glycol 600 as stabilized reagent, (NH<sub>4</sub>)<sub>2</sub>TiF<sub>6</sub> and urea as starting materials at 180 °C. The characterizations show that the TiO<sub>2</sub> hierarchical sphere has well-defined pyramid-shaped crystal facets. The as-prepared TiO<sub>2</sub> hierarchical spheres are crystalline of the anatase phase, with a diameter of about 2–4 μm and a surface area of 36.846 m<sup>2</sup> g<sup>-1</sup>. The optical investigation evidences that the sugar apple-shaped TiO<sub>2</sub> hierarchical sphere film exhibits a prominent light scattering effect at a wavelength range of 600–800 nm due to the unique hierarchical morphology. Furthermore, the sugar apple-shaped TiO<sub>2</sub> hierarchical spheres are deposited as the scattering layer to balance the dye adsorption and light scattering effect in DSSCs and a 7.20% solar energy conversion efficiency is demonstrated, indicating an improvement compared with the P25 cell (6.68%). Based on the optical and electrochemical investigations, the high conversion efficiency is mainly due to the effective suppression of the back reaction of the injected electron with the I<sub>3</sub><sup>-</sup> in the electrolyte and excellent light scattering ability.

Crown Copyright © 2013 Published by Elsevier B.V. All rights reserved.

### 1. Introduction

Since the first report on a low-cost dye-sensitized solar cell (DSSC) in early-1990s by O'Regan and Grätzel [1], it has been received considerable interest as a promising candidate to replace conventional inorganic photovoltaic cell. Until lately, the highest power conversion efficiency of 12.3% has been achieved [2], but this value is still lower than that of bulk silicon solar cells. However, further improvement in DSSC power conversion efficiency still remains a challenge. In recent years, more researchers have focused

attention on improving the efficiency of TiO<sub>2</sub>-based DSSC using nanostructured TiO<sub>2</sub> materials, especially one-dimensional TiO<sub>2</sub> materials (nanowires [3–6], nanorods [7,8] and nanotubes [9,10]), which are believed to gain the enhancement of efficiency because of their rapid electron transfer, reduction of charge recombination degree and enhancement of carrier collection through direct transport pathway. Although one-dimensional TiO<sub>2</sub> materials have been regarded as ideal photoanodes for direct electron transport, the performances of the corresponding DSSCs still lag behind those made of mesoporous nanoparticle photoanodes, due to low specific surface area ascribed to larger diameter and/or free space among the neighboring 1D materials (nanotubes, nanorods or nanowires). As a result, the mesoporous particle-based photoanodes are still the workhorse in DSSC research and the closest to practical application.

\* Corresponding author. Tel./fax: +86 898 31381637.

E-mail address: [sun@hainnu.edu.cn](mailto:sun@hainnu.edu.cn) (Z.-F. Sun).

The overall performance of nanoparticle-based DSSC is still lower than theoretical value due to severe photo-generated electron recombination and poor utilization of near infrared photons. There has been a general consensus that the performance of DSSCs can be further improved by maximizing light harvesting efficiency. To this end, much effort has been dedicated to explore new means to improve light harvesting efficiency [11–22]. The earliest exploited constructions are to incorporate large particles with spherical shape or flat surface into the nanocrystalline TiO<sub>2</sub> matrix or on top of the nanocrystalline TiO<sub>2</sub> layer, which can confine the incident light within the photoanode and increase the optical path of light [15–17]. However, large spherical or flat particles inevitably reduce the surface area of the photoanode and decrease the dye loading. Therefore, it is useful to increase light absorption by scattering effects while maintaining a high surface area of the photoanode for efficient dye adsorption. In recent years, many researchers have made attempts to develop TiO<sub>2</sub> hierarchical microspheres composed of nanoparticles, aiming to provide both high surface area and/or excellent light scattering ability [18–22]. Such TiO<sub>2</sub> microspheres have sub-micrometer or micrometer sizes and thus enhance light scattering ability, while the nanometer-sized building units provide more available surface for dye loading. In spite of the reasonable power conversion efficiency achieved with these TiO<sub>2</sub> hierarchical microspheres, there is still plenty of room for improvements, such as crystallinity, charge transport and dye adsorption capacity.

Herein, we have successfully prepared the sugar apple-shaped TiO<sub>2</sub> hierarchical spheres by a facile hydrothermal method. The hierarchical TiO<sub>2</sub> spheres are around 2–4 μm in size, and possess a surface area of 36.846 m<sup>2</sup> g<sup>-1</sup>. The optical investigation evidences that the sugar apple-shaped TiO<sub>2</sub> hierarchical sphere film has a prominent light scattering effect at a wavelength range of 600–800 nm. Furthermore, we use these sugar apple-shaped TiO<sub>2</sub> hierarchical spheres as the scattering layer to balance the dye adsorption and light scattering effect in DSSCs and a 7.20% solar energy conversion efficiency is demonstrated.

## 2. Experimental section

### 2.1. Preparation of the sugar apple-shaped TiO<sub>2</sub> hierarchical spheres

All chemicals were analytical-grade reagents and were used without further purification. In a typical experimental procedure for the preparation of the sugar apple-shaped TiO<sub>2</sub> spheres, 5.0 mmol (NH<sub>4</sub>)<sub>2</sub>TiF<sub>6</sub> was dissolved into 40.0 mL H<sub>2</sub>O, adding 1.0 mL polyethylene glycol 600 (PEG-600) drop by drop. Subsequently, 45.0 mmol urea was added slowly under stirring. The mixture was kept on stirring for about 30 min to obtain a clear solution, and transferred in a Teflon-lined stainless-steel autoclave (50 mL). Then the autoclave was sealed and maintained at 180 °C for 12 h in an oven. After the reaction, the autoclave was cooled naturally to room temperature. The products were collected and washed with deionized water and ethanol for several times, and finally dried in oven at 50 °C for 6 h.

### 2.2. Characterizations of the sugar apple-shaped TiO<sub>2</sub> hierarchical spheres

The phase purity of the products was characterized by X-ray diffraction (XRD) on a Bruker D8 Advance X-ray diffractometer using Cu K $\alpha$  radiation ( $\lambda=1.5418 \text{ \AA}$ ). The field emission scanning electron microscopy (FE-SEM, JSM-7100F) was performed to characterize the morphology and size. The transmission electron microscopy (TEM) and high-resolution transmission electron microscopy (HRTEM) were performed on a JEOL-2010 HR

transmission electron microscope. To determine the Brunauer–Emmett–Teller (BET) surface area and pore size distribution of the samples, the N<sub>2</sub> sorption measurements were performed by using an Autosorb-iQ surface area analyzer (Quantachrome Instruments US). UV–vis diffuse reflectance spectra and absorption spectra were measured on a UV–Vis–NIR spectrophotometer (UV-1901, Beijing Purkinje General Instrument Co. Ltd., China) to measure the diffuse reflectance of films and dye amounts detached from films, respectively.

### 2.3. Preparation of TiO<sub>2</sub> working electrode

Both pastes of P25 particles (Degussa) and TiO<sub>2</sub> hierarchical spheres were prepared according to Ref. [23]. Briefly, the TiO<sub>2</sub> powder (1.0 g P25 or the as-prepared TiO<sub>2</sub> hierarchical spheres) was ground for 40 min in the mixture of ethanol (8.0 mL), acetic acid (0.2 mL), terpineol (3.0 g) and ethyl cellulose (0.4 g) to form the slurry, and then the slurry was sonicated for 20 min in an ultrasonic bath and finally to form a viscous white TiO<sub>2</sub> paste. The TiO<sub>2</sub> photoanodes were prepared via screen-printing of the above TiO<sub>2</sub> paste on the FTO glass substrate (Nippon Sheet Glass, SnO<sub>2</sub> with sheet resistance of 14 Ω □<sup>-1</sup>). The TiO<sub>2</sub> film thickness could be controlled by repeating the printing number and changing the concentration of the paste. The TiO<sub>2</sub> films were annealed by a calcination process in the furnace through a programmed temperature process (at 325 °C for 5 min, at 375 °C for 5 min, at 450 °C for 15 min, and then at 500 °C for 15 min) to remove the organic compounds.

### 2.4. Fabrication and photovoltaic measurement of DSSCs

The TiO<sub>2</sub> films were immersed in 40.0 mM TiCl<sub>4</sub> solution at 70 °C for 30 min, then calcined at 520 °C for 30 min. After cooling down to ~80 °C, the films were immersed into 0.5 mM N719 dye ([((C<sub>4</sub>H<sub>9</sub>)<sub>4</sub>N]<sub>2</sub>[Ru(II)L<sub>2</sub>(NCS)<sub>2</sub>], where L = 2,2'-bipyridyl-4,4'-dicarboxylic acid, Solaronix SA, Switzerland) in acetonitrile/tert-butanol (volume ratio 1:1) for 16 h at room temperature. Afterward, these films were rinsed with acetonitrile in order to remove physisorbed N719 dye molecules. To evaluate their photovoltaic performances, the dye-sensitized TiO<sub>2</sub>/FTO glass films were sandwiched together with Pt coated FTO glass which was used as the counter electrode. Platinized counter electrodes were fabricated by thermal-deposition of H<sub>2</sub>PtCl<sub>6</sub> solution (5.0 mM in isopropanol) onto FTO glass. The electrolyte, 0.03 M I<sub>2</sub>, 0.6 M 1-methyl-3-propylimidazolium iodide (PMII), 0.10 M guanidinium thiocyanate, and 0.5 M tert-butylpyridine in acetonitrile and valeronitrile (volume ratio 85:15), was introduced from a hole made on the counter electrode into the space between the sandwiched cells.

The photocurrent–voltage characteristics of DSSCs were recorded using a Keithley model 2400 digital source meter under one sun AM 1.5 G (100 mW cm<sup>-2</sup>) illumination with a solar light simulator (Oriel, Model: 94041A). A 450 W Xenon lamp served as a light source and its incident light intensity was calibrated with an NREL-calibrated Si solar cell to approximate AM 1.5 G one sun light intensity before each measurement. The thickness of TiO<sub>2</sub> films was measured by using a D-100 profilometer of KLA-Tencor. The active area of photoanode was 0.16 cm<sup>2</sup>. The electrochemical impedance spectroscopy (EIS) measurements were performed with a Zennium electrochemical workstation (ZAHNER) with the frequency range from 10 mHz to 1000 kHz. The magnitude of the alternative signal was 10 mV. The impedance measurements were carried out under forward bias of –0.83 V in the dark. Incident photon to current conversion efficiency (IPCE) was measured on photo current spectra system of CIMPS (CIMPS-PCS) with tunable light source (TLS03).

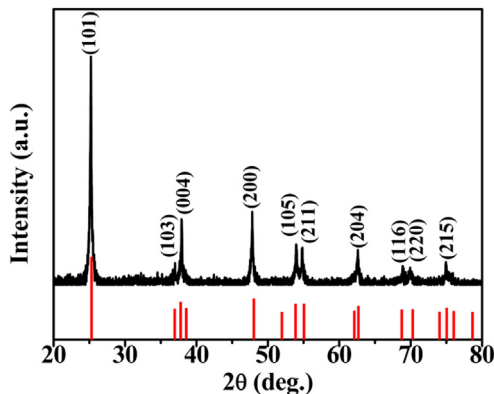


**Fig. 1.** XRD pattern of the as-prepared  $\text{TiO}_2$  hierarchical spheres via a hydrothermal reaction at  $180^\circ\text{C}$  for 12 h.

### 3. Results and discussion

The phase purity and structure of the as-prepared products are characterized by XRD measurement. As shown in Fig. 1, the XRD pattern reveals all diffraction peaks of the as-prepared  $\text{TiO}_2$  hierarchical spheres via a hydrothermal reaction at  $180^\circ\text{C}$  for 12 h can be attributed to pure anatase phase  $\text{TiO}_2$  (JCPDS card No. 78-2486). No characteristic peaks of other phases or impurities are detected. Four main diffraction peaks at  $2\theta$  values of  $25.3^\circ$ ,  $37.8^\circ$ ,  $48.0^\circ$  and  $55.0^\circ$  can be assigned to the (101), (004), (200) and (211) lattice planes of anatase  $\text{TiO}_2$ . The sharp (101) peak of anatase indicates that the as-prepared  $\text{TiO}_2$  sample is highly crystalline after hydrothermal reaction. By using the Debye–Scherrer equation, the crystallite size estimated from the (101) peak is about 19.1 nm. The XRD results confirm that  $\text{TiO}_2$  hierarchical spheres are composed of small anatase nanocrystals.

The unique morphology of as-prepared  $\text{TiO}_2$  hierarchical spheres is revealed by FE-SEM images. The FE-SEM image with low magnification of the as-prepared  $\text{TiO}_2$  products given in Fig. 2a reveals that the samples are spherical objects with diameters in the range of 2–4  $\mu\text{m}$ . In order to show the surface structure clearly, the higher-magnification FE-SEM image in Fig. 2b shows a hierarchical structure with well-defined pyramid-shaped crystal facets. The hierarchical  $\text{TiO}_2$  sphere looks like a sugar apple. It is called ‘sugar apple’ simply because its shape well matches with that of a genuine sugar apple (see Fig. 2d for a comparison of shapes). We further magnify the edge in Fig. 2b and present the image in Fig. 2c. It reveals a uniform surface morphology with well-defined pyramid-shaped crystal facets which have an average edge length of 310 nm, as shown in Fig. 2c.

Detailed morphological and structural information about the as-synthesized sugar apple-shaped  $\text{TiO}_2$  hierarchical spheres is further studied by transmission electron microscopy (TEM). As shown in Fig. 3a, it is clear that the solid microspheres have diameters in the range of 2–4  $\mu\text{m}$ , which is in agreement with the FE-SEM observation. Many flat regions can be easily identified on the external edge of the anatase  $\text{TiO}_2$  microspheres, which are the projection of the pyramid-shaped crystal facets (Fig. 3b and c). As shown in Fig. 3d, it can be measured that the lattice spacing is 0.35 nm, which matches the interplanar distance of (101) planes of anatase  $\text{TiO}_2$ . This result is consistent with the phase structure characterized by XRD (Fig. 1).

Furthermore, the microstructural characteristics of the sugar apple-shaped  $\text{TiO}_2$  hierarchical spheres are further investigated with the  $\text{N}_2$  adsorption–desorption analysis. Fig. 4 shows the nitrogen adsorption–desorption isotherms of the sugar apple-shaped  $\text{TiO}_2$  hierarchical spheres together with the Barret–Joyner–Halenda (BJH) analysis of desorption isotherm in the inset. Fig. 4 exhibits a type IV isotherm with a clear type H3 hysteresis, typical for mesoporous materials. From the  $\text{N}_2$  adsorption–desorption measurements, the Brunauer–Emmett–Teller (BET)

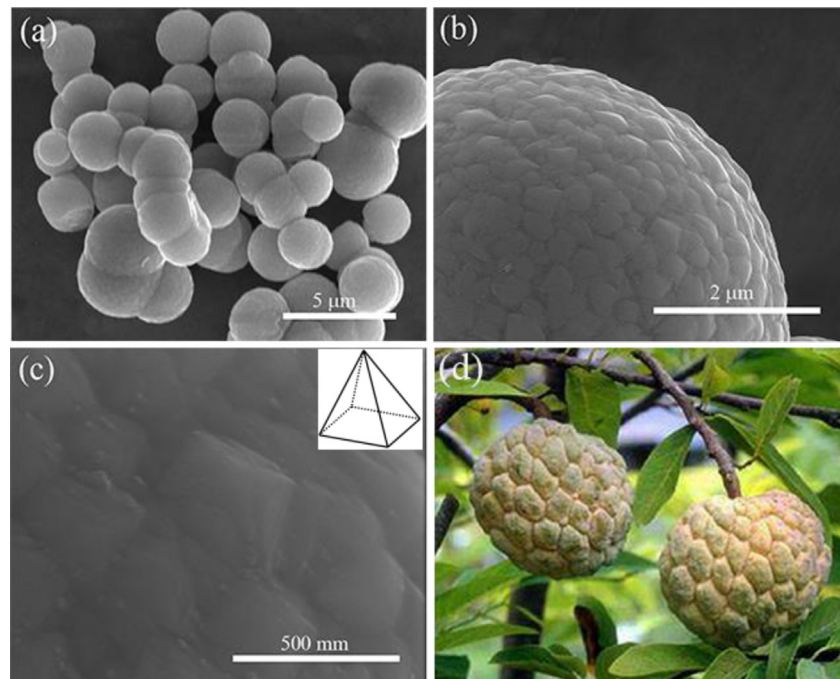


**Fig. 2.** FE-SEM images of the as-synthesized sugar apple-shaped  $\text{TiO}_2$  hierarchical spheres (a, b, c). Digital image of genuine sugar apple (d). The inset is schematic diagram of an individual pyramid-shaped structure.

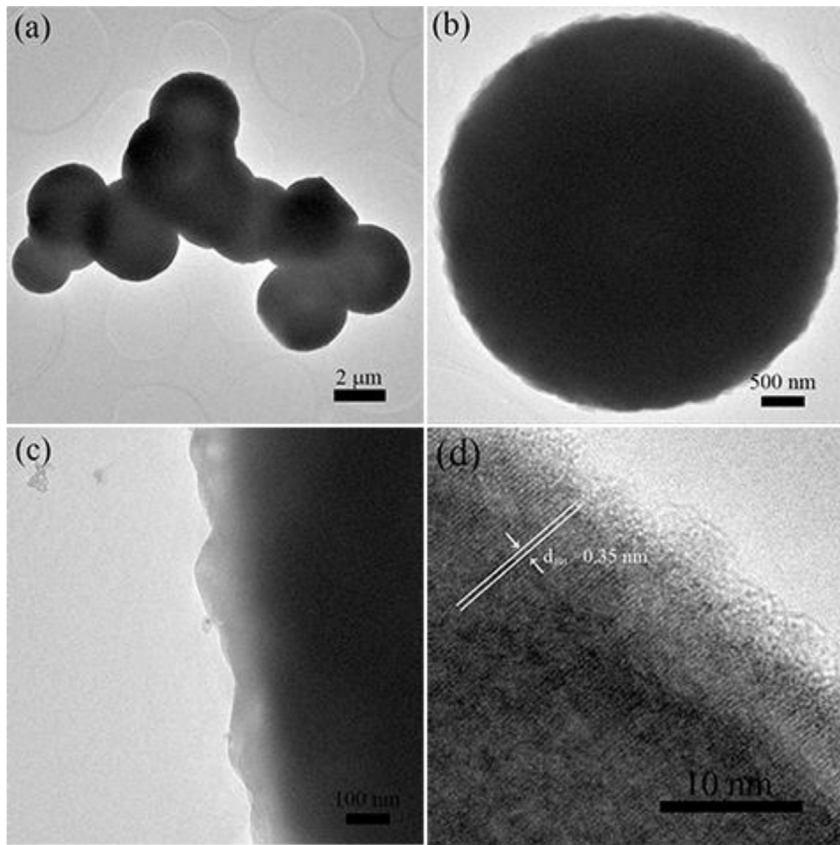


**Fig. 3.** TEM (a, b, c) and HRTEM (d) images of the as-prepared hierarchical  $\text{TiO}_2$  spheres.

surface area of the sugar apple-shaped  $\text{TiO}_2$  hierarchical spheres is  $36.846 \text{ m}^2 \text{ g}^{-1}$ , which is much lower than that of P25 ( $54.214 \text{ m}^2 \text{ g}^{-1}$ ). According to the Barret–Joyner–Halenda (BJH) model, it can be seen that the sugar apple-shaped  $\text{TiO}_2$  hierarchical spheres possess small mesopores peaking at 1.9 and 4.8 nm calculated from the desorption branch of the isotherm (inset in Fig. 4).

In order to investigate the scattering effect of the sugar apple-shaped  $\text{TiO}_2$  hierarchical spheres on the photovoltaic performance, we compared three types of cells with different film structures. Two films composed of a single layer of commercial  $\text{TiO}_2$

nanocrystals (P25, Degussa) and the sugar apple-shaped  $\text{TiO}_2$  hierarchical spheres with the same thickness of  $16 \mu\text{m}$  were labeled as film-1 and film-2, respectively. The sugar apple-shaped  $\text{TiO}_2$  hierarchical spheres were deposited as the scattering layer ( $4 \mu\text{m}$ ) on the commercial P25 film ( $12 \mu\text{m}$ ) to fabricate the bilayer film which was labeled as film-3. Fig. 5 displays the cross-sectional FE-SEM images of these films. Moreover, the corresponding DSSCs assembled from these films were denoted as cell-1, cell-2 and cell-3, respectively.

The photocurrent density–voltage ( $J$ – $V$ ) curves of DSSCs based on the three types of films (cell-1: film-1; cell-2: film-2 and cell-3: film-3) are shown in Fig. 6, and their detailed photovoltaic parameters derived from the  $J$ – $V$  curves are summarized in Table 1. As shown in Fig. 6 and Table 1, the fill factor (FF) of the DSSCs based on three films doesn't show any obvious changes. It can be seen that both the  $V_{\text{oc}}$  of the cell-2 ( $V_{\text{oc}} = 0.851 \text{ V}$ ) and cell-3 ( $V_{\text{oc}} = 0.845 \text{ V}$ ) are comparatively higher than that obtained from the cell-1 ( $V_{\text{oc}} = 0.823 \text{ V}$ ). The higher  $V_{\text{oc}}$  of the cell-2 and cell-3 employing the sugar apple-shaped  $\text{TiO}_2$  hierarchical spheres suggests that the recombination between the electrons in the  $\text{TiO}_2$  hierarchical sphere electrode and  $\text{I}_3^-$  in the electrolytes is suppressed due to the smaller surface area of the  $\text{TiO}_2$  hierarchical sphere electrode compared with that of the commercial P25 electrode [24]. Besides, from the dark current measurement of the three cells in Fig. 7, we could see the dark current of cell-2 based on  $\text{TiO}_2$  hierarchical spheres is the lowest. With the decrease of the dark current, the charge recombination between transferred electrons and  $\text{I}_3^-$  could be reduced and the  $V_{\text{oc}}$  is improved. As a result of less recombination, the photoelectrodes containing the sugar apple-shaped  $\text{TiO}_2$  hierarchical spheres increase  $V_{\text{oc}}$ . However, cell-2 displays a lower  $J_{\text{sc}}$  value of  $9.11 \text{ mA cm}^{-2}$  than the  $J_{\text{sc}}$  value of  $11.45 \text{ mA cm}^{-2}$ .

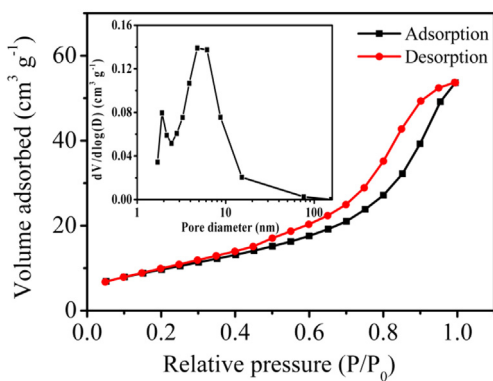


**Fig. 4.** Nitrogen adsorption–desorption isotherms of the sugar apple-shaped  $\text{TiO}_2$  hierarchical spheres. The inset shows Barret–Joyner–Halenda (BJH) pore size distribution plot of the sugar apple-shaped  $\text{TiO}_2$  hierarchical spheres.

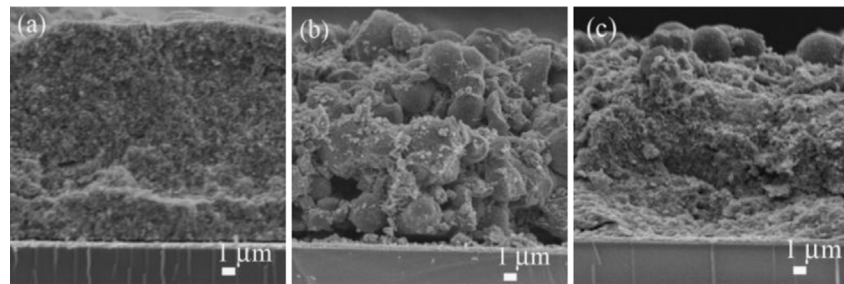


**Fig. 5.** Cross-sectional FE-SEM images of film-1 (a), film-2 (b) and film-3 (c).

for cell-1. These results lead to a low  $\eta$  value of 5.09% for cell-2, while the  $\eta$  value of cell-1 is 6.68%. When the as-prepared sugar apple-shaped  $\text{TiO}_2$  hierarchical spheres are deposited to form a scattering layer, the  $J_{sc}$  value of cell-3 is increased to  $12.17 \text{ mA cm}^{-2}$  and the  $\eta$  value of cell-3 was improved to 7.20%, which should be the result of the better light scattering ability of the sugar apple-shaped  $\text{TiO}_2$  hierarchical spheres.

It is well-known that the  $J_{sc}$  depends on the charge harvesting efficiency ( $\eta_{lh}$ ), the charge-injection efficiency ( $\eta_{inj}$ ) and the charge collection efficiency ( $\eta_{cc}$ ) by the expression [25]:  $J_{sc}=q\eta_{lh}\eta_{inj}\eta_{cc}I_0$  ( $q$  is the elementary charge,  $I_0$  is light flux). Here, the  $\eta_{inj}$  is assumed to be the same for the three DSSCs because of the same dye (N719) adsorbed on the same semiconductor material ( $\text{TiO}_2$ ). The  $\eta_{lh}$  relates to the dye loading and light scattering ability. Hierarchical spheres have been proven to enhance the light scattering effect, hence leading to higher photocurrent and photovoltaic performance. In order to investigate the light scattering property of the three films, the UV-vis reflectance spectra are further characterized and shown in Fig. 8. The commercial P25 film (film-1) fabricated from nanometer-sized crystallites exhibits a weak scattering effect and large amounts of visible light in the long wavelength region transmitted through the film directly, whereas the sugar apple-shaped  $\text{TiO}_2$  hierarchical sphere film (film-2) shows much stronger reflectance. This can be explained by light scattering of the sugar apple-shaped  $\text{TiO}_2$  hierarchical spheres, because the particle size of the  $\text{TiO}_2$  hierarchical microsphere is analogous to the wavelength of visible light it can lead to a strong scattering effect according to Mie theory [26]. This result illustrates that the sugar apple-shaped  $\text{TiO}_2$  hierarchical spheres have more suitable structure for light scattering than the P25 nanocrystallites. The bilayer film (film-3) consists of both P25 nanocrystallites and  $\text{TiO}_2$  hierarchical spheres, and therefore the intensity of diffuse reflectance of it falls between the sugar apple-shaped  $\text{TiO}_2$  hierarchical sphere film (film-2) and P25 film (film-1).

The dye loading results (UV-vis absorption) show that the amount of dye adsorbed on the as-prepared sugar apple-shaped  $\text{TiO}_2$  hierarchical sphere film (film-2:  $9.11 \times 10^{-8} \text{ mol cm}^{-2}$ ) is almost twice lower than that of the commercial P25 film (film-1:  $18.75 \times 10^{-8} \text{ mol cm}^{-2}$ ). This result is reasonable, because the surface area of the commercial P25 nanoparticles is larger than that

of the sugar apple-shaped  $\text{TiO}_2$  hierarchical spheres when the thickness of films is same. In comparison with cell-2, cell-1 shows a higher  $J_{sc}$ , attributed to adsorb larger amounts of dye molecules. Compared to cell-1, cell-3 had a higher  $J_{sc}$ , although the cell-3 adsorbed lower amounts of dye molecules than that of the cell-1, the greater scattering effect of the sugar apple-shaped  $\text{TiO}_2$  hierarchical spheres compensated for this, leading to enhance  $\eta$  of cell-3.

Fig. 9 displays the incident photon to current efficiency (IPCE) spectra as a function of wavelength for three cells. Compared to cell-1, cell-2 exhibits a lower IPCE which should be a result of the lower amount of dye anchored onto the sugar apple-shaped  $\text{TiO}_2$  hierarchical sphere film. In comparison with cell-1, cell-3 possesses higher IPCE value even with less dye adsorbed. This result further confirmed that the light scattering effect of the sugar apple-shaped  $\text{TiO}_2$  hierarchical spheres is stronger than that of P25 nanoparticles. It is worth noting that the IPCE data of cell-2 and cell-3 show an obvious red-shift to a longer wavelength (600–800 nm) compared to the cell-1 due to the better light scattering ability for the sugar apple-shaped  $\text{TiO}_2$  hierarchical spheres. This result is in agreement with the  $J_{sc}$  data displayed in Table 1.

Electrochemical impedance spectroscopy (EIS) has been regarded as a powerful technique to characterize the electron transport and recombination processes in DSSC. Generally, three characteristics semicircles can be obtained from EIS spectra in the frequency range between  $10^6 \text{ Hz}$  and  $10^{-2} \text{ Hz}$ . The high-frequency semicircle corresponds to the charge-transfer resistance at the interface of the counter electrode and the electrolyte ( $R_{ct1}$ ). The middle-frequency semicircle is related to electron transfer and recombination at the  $\text{TiO}_2$ /dye/electrolyte interfaces ( $R_{ct2}$ ). The low-frequency semicircle corresponds to Nernst diffusion of  $\text{I}^-/\text{I}_3^-$  within the electrolyte ( $Z_w$ ) [27,28]. Fig. 10 shows the impedance spectra of three cells. The

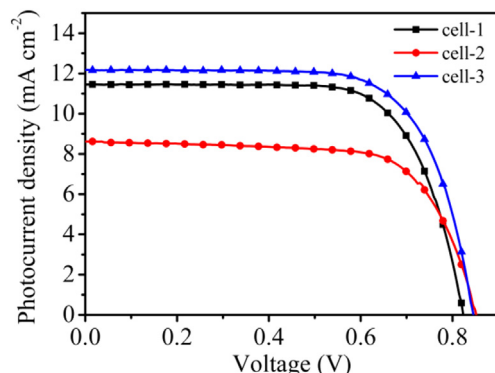


**Fig. 6.** The photocurrent–voltage curves of the DSSCs based on different working electrodes (film-1, film-2, and film-3) measured under the illumination of one sun (AM 1.5 G,  $100 \text{ mW cm}^{-2}$ ).

**Table 1**

Detailed photovoltaic parameters of cells based on film-1, 2 and 3 measured under AM 1.5 G one sun illumination.  $J_{sc}$ : short-circuit photocurrent density;  $V_{oc}$ : open-circuit photovoltage; FF: fill factor;  $\eta$ : photovoltaic conversion efficiency.

Cell	Dye absorption ( $\times 10^{-8} \text{ mol cm}^{-2}$ )	$J_{sc}$ ( $\text{mA cm}^{-2}$ )	$V_{oc}$ (V)	FF (%)	$\eta$ (%)
Cell-1	18.75	11.45	0.823	70.9	6.68
Cell-2	9.11	8.61	0.851	69.5	5.09
Cell-3	13.66	12.17	0.845	71.2	7.20

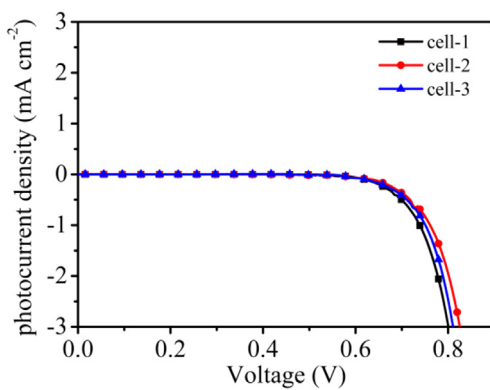


**Fig. 7.** The plots of dark current as a function of applied bias for three DSSCs.

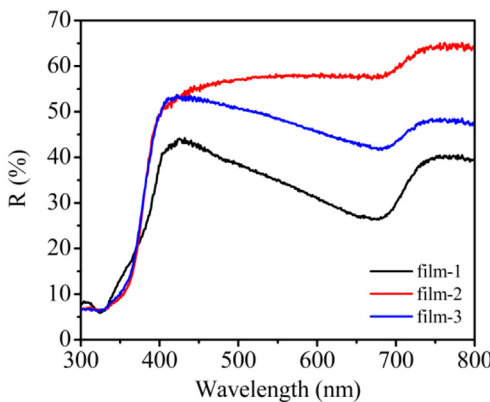


**Fig. 8.** Diffuse reflectance spectra of the three films.

resistance values are fitted by Z-view software using an equivalent circuit containing resistance ( $R$ ) and constant phase element ( $CPE$ ), and the simulated parameters are summarized in **Table 2**. The three cells show similar  $R_s$  and  $R_{ct1}$ , leading to similar fill factors because the same electrolyte and counter electrode are used. However, the  $R_{ct2}$  value of cell-1, cell-2 and cell-3 is 85.21, 165.6 and 149.4  $\Omega$ , respectively. This result indicates that cell-2 has a slower electron recombination process, that is, a more effective suppression of the back reaction of the injected electron with the  $I_3^-$  in the electrolyte in cell-2. The product of the charge-transfer resistance and the chemical capacitance corresponds to the electron lifetime,  $\tau = CPE \times R$ , we are able to extract information on electron lifetime. The  $\tau$  value of cell-2, cell-3 and cell-1 is 242, 140 and 100 ms, respectively. The longer electron lifetime for the sugar apple-shaped  $TiO_2$

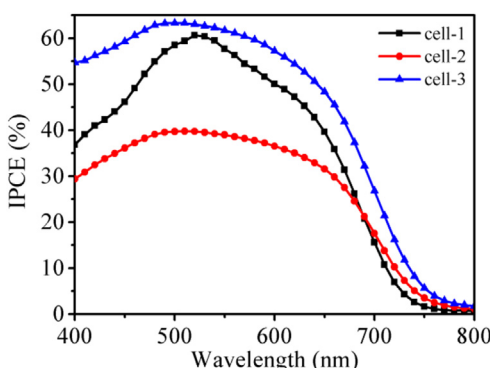


**Fig. 9.** Incident photon to current conversion efficiency (IPCE) curves of DSSCs based on different working electrodes (film-1, film-2, and film-3).

**Table 2**

Series resistance ( $R_s$ ), charge transfer resistance ( $R_{ct1}$ ), and electron transfer and recombination ( $R_{ct2}$ ) of the DSSCs fabricated using different photoanodes.

Cell	$R_s$ ( $\Omega$ )	$R_{ct1}$ ( $\Omega$ )	$R_{ct2}$ ( $\Omega$ )	$\tau$ (ms)
Cell-1	11.05	8.68	85.21	100
Cell-2	11.66	5.76	165.6	242
Cell-3	11.74	6.59	149.4	140

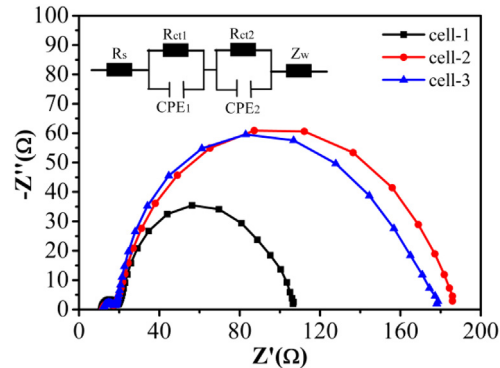


**Fig. 10.** The electrochemical impedance spectra of DSSCs based on different photoanodes measured in the dark at  $-0.83$  V bias. And the inset illustrates the equivalent circuit simulated to fit the impedance spectrum.

hierarchical spheres based DSSC (cell-2) also further supports its higher  $V_{oc}$ . This result agrees well with the  $J-V$  data (**Fig. 6**).

#### 4. Conclusions

In summary, we have successfully synthesized the sugar apple-shaped  $TiO_2$  hierarchical spheres by a facile hydrothermal method with PEG-600 as stabilized reagent,  $(NH_4)_2TiF_6$  and urea as starting materials at  $180$  °C for 12 h. The as-prepared  $TiO_2$  hierarchical spheres are crystalline of the anatase phase, with a diameter of about 2–4  $\mu m$  and a surface area of  $36.846\text{ m}^2\text{ g}^{-1}$ . The optical investigation evidences that the sugar apple-shaped  $TiO_2$  hierarchical sphere film has a prominent light scattering effect at a wavelength range of 600–800 nm. The hierarchical structure allows more efficient transport for electrolytes and enhances the light scattering effect. Furthermore, we use these sugar apple-shaped  $TiO_2$  hierarchical spheres as the scattering layer to balance the dye adsorption and light scattering effect in DSSCs and a 7.20% solar energy conversion efficiency is obtained. The efficiency of DSSCs made from the sugar apple-shaped  $TiO_2$  hierarchical spheres as the scattering layer is higher than that of DSSC made from the monolayer P25 due to the effective suppression of the back reaction of the injected electron with the  $I_3^-$  in the electrolyte and excellent light scattering ability.

#### Acknowledgements

This work is supported by the Nature Science Foundation of Hainan Province (212013), the Foundation of Hainan Normal University and the Undergraduate Training Programs for Innovation and Entrepreneurship (cxcyxj2013006).

#### References

- [1] B. O'Regan, M. Grätzel, *Nature* 353 (1991) 737–740.
- [2] A. Yella, H.W. Lee, H.N. Tsao, C.Y. Yi, A.K. Chandran, M.K. Nazeeruddin, E.W.G. Diau, C.Y. Yeh, S.M. Zakeeruddin, M. Grätzel, *Science* 334 (2011) 629–634.
- [3] P.P. Sun, X.T. Zhang, X.P. Liu, L.L. Wang, C.H. Wang, J.K. Yang, Y.C. Liu, J. Mater. Chem. 22 (2012) 6389–6393.

- [4] J.Y. Liao, B.X. Lei, H.Y. Chen, D.B. Kuang, C.Y. Su, *Energy Environ. Sci.* 5 (2012) 5750–5757.
- [5] X.J. Feng, K. Shankar, O.K. Varghese, M. Paulose, T.J. Latempa, C.A. Grimes, *Nano Lett.* 8 (2008) 3781–3786.
- [6] X.Y. Wang, Y. Liu, X. Zhou, B.J. Li, H. Wang, W.X. Zhao, H. Huang, C.L. Liang, X. Yu, Z. Liu, H. Shen, *J. Mater. Chem.* 22 (2012) 17531–17538.
- [7] B. Liu, E.S. Aydil, *J. Am. Chem. Soc.* 131 (2009) 3985–3990.
- [8] M.Q. Lv, D.J. Zheng, M.D. Ye, L. Sun, J. Xiao, W.X. Guo, C.J. Lin, *Nanoscale* 4 (2012) 5872–5879.
- [9] B.X. Lei, J.Y. Liao, R. Zhang, J. Wang, C.Y. Su, D.B. Kuang, *J. Phys. Chem. C* 114 (2010) 15228–15233.
- [10] F.W. Zhuge, J.J. Qiu, X.M. Li, X.D. Gao, X.Y. Gan, W.D. Yu, *Adv. Mater.* 23 (2011) 1330–1334.
- [11] J.G. Yu, J.J. Fan, L. Zhao, *Electrochim. Acta* 55 (2010) 597–602.
- [12] J.G. Yu, J.J. Fan, K.L. Lv, *Nanoscale* 2 (2010) 2144–2149.
- [13] J.G. Yu, Q.L. Li, Z. Shu, *Electrochim. Acta* 56 (2011) 6293–6298.
- [14] J.G. Yu, J.J. Fan, B. Cheng, *J. Power Sources* 196 (2011) 7891–7898.
- [15] S. Hore, C. Vetter, R. Kern, H. Smit, A. Hinsch, *Sol. Energy Mater. Sol. Cells* 90 (2006) 1176–1188.
- [16] Z.S. Wang, H. Kawauchi, T. Kashima, H. Arakawa, *Coord. Chem. Rev.* 248 (2004) 1381–1389.
- [17] J.H. Yoon, S.R. Jang, R. Vittal, J. Lee, K.J. Kim, *J. Photochem. Photobiol., A: Chem.* 180 (2006) 184–188.
- [18] Y.J. Kim, M.H. Lee, H.J. Kim, G. Lim, Y.S. Choi, N.G. Park, K. Kim, W.I. Lee, *Adv. Mater.* 21 (2009) 3668–3673.
- [19] W.G. Yang, F.R. Wan, Q.W. Chen, J.J. Li, D.S. Xu, *J. Mater. Chem.* 20 (2010) 2870–2876.
- [20] D.H. Chen, F.Z. Huang, Y.B. Cheng, R.A. Caruso, *Adv. Mater.* 21 (2009) 2206–2210.
- [21] H.J. Koo, Y.J. Kim, Y.H. Lee, W.I. Lee, K. Kim, N.G. Park, *Adv. Mater.* 20 (2008) 195–199.
- [22] J.Y. Liao, B.X. Lei, D.B. Kuang, C.Y. Su, *Energy Environ. Sci.* 4 (2011) 4079–4085.
- [23] B.X. Lei, W.J. Fang, Y.F. Hou, J.Y. Liao, D.B. Kuang, C.Y. Su, *J. Photochem. Photobiol., A: Chem.* 216 (2010) 8–14.
- [24] J.H. Park, S.Y. Jung, R. Kim, N.G. Park, J. Kim, S.S. Lee, *J. Power Sources* 194 (2009) 574–578.
- [25] K. Zhu, N.R. Neale, A. Miedaner, A.J. Frank, *Nano Lett.* 7 (2007) 69–74.
- [26] F.Z. Huang, D.H. Chen, X.L. Zhang, R.A. Caruso, Y.B. Cheng, *Adv. Funct. Mater.* 20 (2010) 1301–1305.
- [27] D.B. Kuang, C. Klein, Z.P. Zhang, S. Ito, J.E. Moser, S.M. Zakeeruddin, M. Grätzel, *Small* 3 (2007) 2094–2102.
- [28] B.X. Lei, Q.P. Luo, X.Y. Yu, W.Q. Wu, C.Y. Su, D.B. Kuang, *Phys. Chem. Chem. Phys.* 14 (2012) 13175–13179.